OCEANS Conference 2022 - Chennai

Spectral Ultrasonic Underwater Buried Object Detection and Localization

Fabian John*, Sven Ole Schmidt*, Horst Hellbrück*†
*Technische Hochschule Lübeck - University of Applied Sciences, Germany
Department of Electrical Engineering and Computer Science, Center of Excellence CoSA
Email: fabian.john@th-luebeck.de, sven.ole.schmidt@th-luebeck.de, horst.hellbrueck@th-luebeck.de
† University of Luebeck, Germany, Institute of Telematics

***Abstract*—Acoustic object detection in underwater applications, such as the detection of unexploded ordnances (UXO), is challenging, especially at shallow burial depths or in the presence of other reflections. Therefore, acoustic detection is performed with very short temporal and spectrally very broadband pulses. The received signal strength is measured and displayed over time (time of flight). However, this method cannot detect closely spaced reflections because the pulses overlap in the time domain. In this work, we present spectral signal processing that allows the detection and localization of known object geometries in the presence of interfering reflections. We extend our underwater ultrasound propagation model in this work to include a sediment layer. We apply spectral fingerprinting to detect a known object geometry and localize it in a second step. We evaluate the performance with measurements in a laboratory experiment with an object with varying burial depths and on sediment.**

***Index Terms*—acoustic, object detection, spectral, unexploded ordnances (UXO), underwater, ultrasonic, wideband pulse**

I. Introduction

Acoustic systems have a wide range of applications in the underwater sector, e.g., for localization, object detection, or communication. Ultrasonic transducers and signal processing hardware are available for these systems in many variants and allow optimal and cost-efficient development.

Acoustic detection of unexploded ordnance (UXO) buried in sediment is an unsolved problem, especially at shallow burial depths. The multipath propagation of ultrasonic waves, including scattering, reflection, diffraction, and doppler effects, is a challenging task in acoustic underwater applications, such as communication and object localization [1], [2], [3], [4]. Acoustic pulse-echo systems, such as subbottom profilers, are used to detect objects in sediment [5], [6]. However, pulse-echo systems require a minimum distance of at least one pulse length between different reflectors to detect them with the time of flight (TOF) measurements. Therefore, wideband pulses are used in such systems because they are very short in the time domain. The TOF is evaluated by the envelope of the received signal [7], [8], [9], [10].

As ultrasonic waves propagate with different attenuation, velocities, and frequencies on each multipath [1], [11], [12], this work presents spectral signal processing for pulse-echo systems for improved detection and localization of objects buried in sediment. Based on our ultrasonic underwater propagation model, we present the extension of the model with a sediment layer [13]. Our model considers reflections and diffraction components and calculates the received signal for known geometries and arrangements. The original model is based on the multipath propagation model, with knife-edge diffraction calculated via Fresnel integrals, for device-free localization with electromagnetic ultrawideband pulses [14], [15]. For detection and localization, we perform a fingerprinting procedure based on the nearest neighbor algorithm [16]. To the best of our knowledge, diffraction effects are not yet utilized in a spectral approach to improve localization of objects although they were identified as a source of disturbances in underwater communication and localization tasks [17], [7], [18], [5].

The components for automated measurement and signal processing are set up as a distributed system. The distributed measurement system and our automated precision 3D positioning system were presented at the Oceans Conference 2021 - San Diego, Porto [19], [20].

The contributions of the paper are:

- We present our extended spectral underwater ultrasonic propagation model.
- We show the model-based detection and localization of a known buried object geometry by applying the nearest neighbor algorithm.
- We evaluate our advanced spectral object detection approaches with measurements performed in a laboratory aquarium with an object buried in varying depths.

OCEANS Conference 2022 - Chennai

The paper is structured as follows. First, we describe our underwater ultrasonic propagation model and the extension with a sediment layer for fingerprint-based object detection and localization. We then describe our spectral model-based method for visualizing and highlighting a searched object. We subsequently describe the setup used for the evaluation measurements and explain how the experiments were conducted. Finally, we present the results of the measurements performed for evaluation and summarize the results.

II. Extended Spectral Underwater Ultrasonic Propagation Model

We apply and extend our model to calculate the spectral received signal of a transmitted ultrasonic pulse in the presence of an object [13]. We have already validated this model for multipath propagation in free water. In the following, we present the geometry of the model used and the extensions necessary to model the objects buried in the sediment.

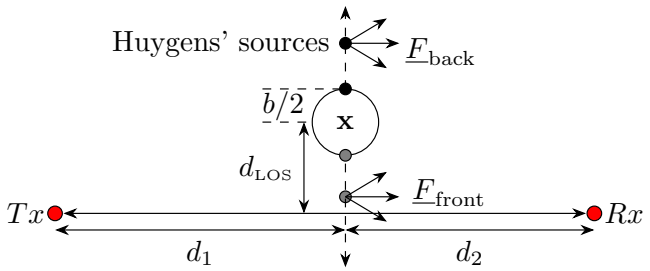

Figure 1. Geometry of the spectral ultrasonic multipath propagation model [13] (©2021 IEEE).

In the original model, an object with a circular cross-section was placed perpendicular to the line-of-sight (LOS) connection between an ultrasonic transmitter and receiver (see Figure 1). The omnidirectional ultrasonic wave emitted by the transmitter is transmitted at the receiver in a direct path (LOS connection). In addition, the emitted wave is diffracted at the object, and in the receiver, this signal is also received. Since the propagation path of the diffraction component around the object is larger than the direct line-of-sight connection, the received signals of the two path components arrive phase-shifted. By applying broadband ultrasonic pulses, we have already shown with our spectral multipath propagation model that object position in open water is precisely determined with fingerprinting [13].

The spectrum of pulses overlapping in the time domain is applied for position determination with the presented method. Our model is not applicable for non-overlapping pulses in the time domain, whereas time-of-flight methods are already applied successfully for this application. In this paper, we present the application of our method in addition to time-of-flight representations to highlight overlapping pulses of an object and the sediment-water transition.

As mentioned above, a temporal overlap of the received multipath components is necessary to form the spectral patterns. In real exploration scenarios, we assume that the distance between ultrasound transmitter and receiver is small compared to the distance to the sediment and that the LOS component does not overlap in time with the multipath components of the buried object and the water-sediment transition. We accounted for this accordingly in our modeling and measurements in the laboratory.

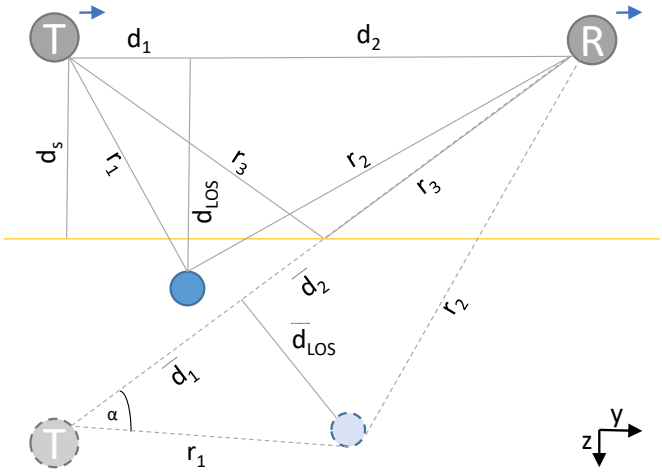

Figure 2. Geometry of the adapted spectral ultrasonic multipath propagation model for buried objects.

Figure 2 shows the adapted spectral ultrasonic multipath propagation model for buried objects. To ensure that the LOS propagation component does not interfere with the others, the condition

$$d_1 + d_2 < 2 \cdot r_3 - T_{pulse} \cdot c \tag{1}$$

must be satisfied, where the propagation velocity c, the pulse duration T_{pulse} and the distance to the sediment d_s must be known. With the condition in Equation 1, the geometry can be transformed according to the Figure 2. Propagation along the LOS via d_1 and d_2 arrives independently in time from the multipath components of the sediment-water transition via $2 \cdot r_3$ and diffraction from the object via r_1 and r_2. In contrast, the multipath components of the sediment-water transition and diffraction at the object are assumed to overlap in time. Geometrically, we model the propagation paths by mirroring the transmitter at the water-sediment edge as a virtual source (dashed) and place a virtual object (dashed) so that the propagation path corresponds to the original $r_1 + r_2$. From the given quantities d_1, d_2, d_s, d_{LOS}, the unknown r_1, r_2, r_3, α, $\bar{d}_{LOS}$, $\bar{d}_1$ and $\bar{d}_2$ are determined using Equation 2 - 8 via the Pythogorean theorem, the sine theorem and cosine theorem.

$$r_1 = \sqrt{d_1^2 + d_{LOS}^2} \tag{2}$$

$$r_2 = \sqrt{d_2^2 + d_{LOS}^2} \tag{3}$$

$$r_3 = \sqrt{\frac{(d_1 + d_2)^2}{4} + d_s^2} \tag{4}$$

$$\alpha = \arccos \frac{r_1^2 + (2 \cdot r_3)^2 - r_2^2}{2 \cdot r_1 \cdot (2 \cdot r_3)} \tag{5}$$

OCEANS Conference 2022 - Chennai

$$\overline{d}_{LOS} = r_1 \cdot \sin\alpha \tag{6}$$

$$\overline{d}_1 = \sqrt{r_1^2 - \overline{d}_{LOS}^2} \tag{7}$$

$$\overline{d}_2 = \sqrt{r_2^2 - \overline{d}_{LOS}^2} \tag{8}$$

With the parameters $\overline{d}_{LOS}$, $\overline{d}_1$ and $\overline{d}_2$ we calculate the received spectrum for the sediment-water component and diffraction at the object with our model. To account for the 180° phase shift that occurs at the reflection on the water-sediment transition, we introduced a factor of -1 to the model's Fresnel components. The modeled spectral received signal for for a buried object with $d_1 + d_2 = 14$ cm, $d_s = 17$ cm and $d_{LOS} = 20$ cm, for the transmitter and receiver moved across the buried object (from left to right in Figure 2, indicated by the arrows) is shown in Figure 3.

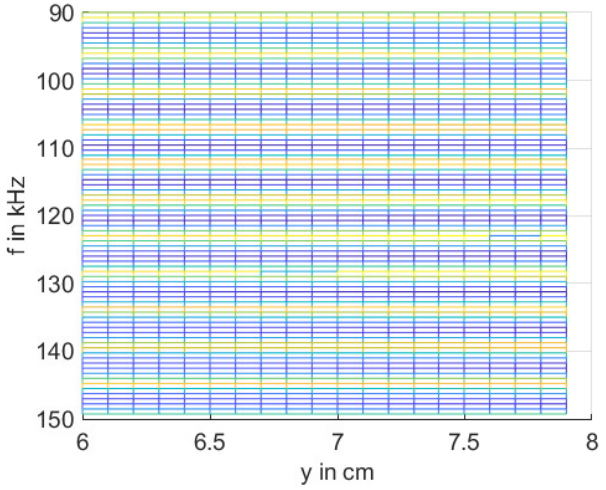

Figure 3. Modeled spectrum of a buried object, by moving the sensors across in y direction.

The spectrum model provides results for a range of d_{LOS} that highlight the object position in the time-of-flight representation in the measured data, as described in Section III.

III. Spectral Model Based Highlighting

With the model presented in Section II, we calculate the spectrum for a received ultrasonic pulse where the propagation component of the water-sediment transition and the diffraction component at a buried object overlap. Assuming that the distance d_s of our measurement system to the water-sediment transition is known, we calculate the spectra (as exemplified in Figure 3 for a d_{LOS}) for a range of d_{LOS}. From this, we obtain a spectral fingerprint for each of the object's varying burial depths. These calculated fingerprints are compared with the data measured in the laboratory experiment via the calculation of the correlation with a shift of zero [21]. In Figure 4(a) the envelope of the received signal for measurement with the buried object is shown. In the region of reflection at the water-sediment transition at $z = 20$ cm, we calculate the measured spectra below for two-dimensional windows of size $b_y = 2$ cm and $b_z = 2$ cm. Figure 4(b) shows an exemplary window (yellow colored) for the depicted envelope. This window is moved in $dy = 0.1$ cm and $dz = 0.4$ cm through a region of interest (ROI) of the measurement and the spectrum (two-dimensional) is calculated for each window.

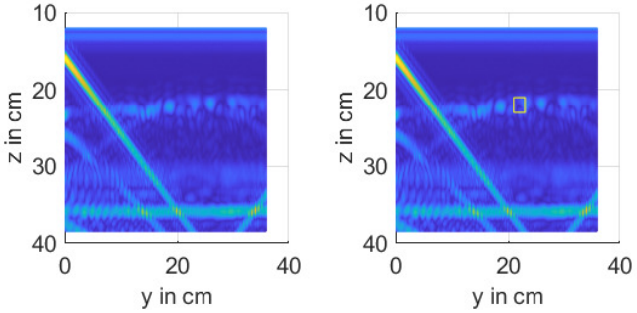

(a) Measured envelope. (b) Measured envelope with window.

Figure 4. Time domain representaion of the measurement of buried object.

The calculated spectrum for the window shown in Figure 4(b) is shown in Figure 5. For each spectrum of the windows of the measurement, the similarity Δ to the corresponding modeled spectrum is determined by the integral of the punctual multiplication between the spectra according to Equation 9. By calculating with Equation 9 the qualitative similarity of the spectra, which cannot be evaluated visually, is calculated.

$$\Delta_{y_{\text{win}}, z_{\text{win}}} = \int\int Y_{\text{Model}}(f, y) \cdot Y_{\text{Measurement}}(f, y)\, df\, dy \tag{9}$$

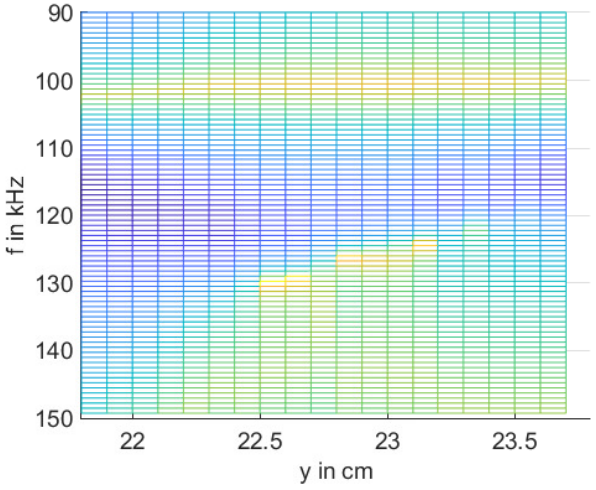

Figure 5. Measured spectrum of a buried object for an exemplary window.

In the following step, the calculated similarity is multiplied by the value of the envelope in the time domain in the respective window center with Equation 10.

$$y_{\text{Highlited}}(y, z) = y_{\text{Measurement}}(y, z) \cdot (B \cdot \Delta_{y,z})^A \tag{10}$$

OCEANS Conference 2022 - Chennai

Here, the factors A and B are chosen accordingly to adjust the intensity of the highlighting. In our evaluation in Section IV the factor $A = 2$ was chosen, and B was calculated according to the maximum of Δ that amplification by the factor of maximum 9 occurs in the highlighting. In Figure 8, the envelope is shown in the top row and the envelope post-processed with spectral highlighting is shown in the bottom row.

IV. Evaluation Setup

Table I lists the measurement parameters.

To evaluate our model-based fingerprinting for object detection and localization, we perform measurements with a hollow cylindrical object at different burial depths and place it on the sediment (Figure 6 position 1).

Measurements were performed in a laboratory aquarium with a size of $60\ \mathrm{cm} \times 80\ \mathrm{cm} \times 60\ \mathrm{cm}$. The transducers are moved around the aquarium in an automated manner using a precision 3D positioning system [19]. A RedPitaya generates and acquires the analog signals. It drives the transducers, which can be controlled automatically via the message queue telemetry transport (MQTT) protocol [20]. The measurement setup with the two transducers (shown in Position 5) attached to the automatic 3D positioning system and the buried cylinder are shown in Figure 6 for six different burial depths. The buried object was equipped with a vertical rod on each side, on which corresponding markings show the burial depth (see Figure 7). During the measurements, the burial depth of the object was manually changed step by step. Position changes of buried objects cannot be automated in our laboratory, so the variation of burial depths between measurements is not uniform (see Figure 8).

In each position, the transducers were moved in steps of $0.1\ \mathrm{cm}$ horizontally (y-direction) across the object and a single pulse was transmitted and received in each step. The vertical position (in z direction) was static for all the measurements.

The measurements were performed with TC4013 hydrophone transducers from Teledyne Marine in the given frequency range [22]. The transducers were driven and digitized via a self-designed PCB ultrasonic audio power amplifier with a gain factor of 10 using a RedPitaya 125-14 [9]. Raw measured values were transferred from RedPitaya to a PC via the MQTT protocol, spectrally processed further and the result stored.

TABLE I
Meseaurement parameters for the evaluation.

Parameter	Value	Description
b	$2.7\ \mathrm{cm}$	Obstacle diameter
$d_1 + d_2$	$14\ \mathrm{cm}$	LOS distance to transducers
d_s	$17\ \mathrm{cm}$	Perpendicular distance sensors to sediment
d_{LOS}	$17 - 22\ \mathrm{cm}$	Perpendicular obstacle distance
y	$0 - 36\ \mathrm{cm}$	Moving distance across the object
f_{pulse}	$90\ \mathrm{kHz}$	Lower frequency bound
f_{high}	$150\ \mathrm{kHz}$	Upper frequency bound
c	$1503\ \mathrm{m/s}$	Velocity of sound
T_{pulse}	$110\ \mu\mathrm{s}$	Length of transmitted pulse
$L \times W \times H$	$80\ \mathrm{cm} \times 60\ \mathrm{cm} \times 60\ \mathrm{cm}$	Lab. tank Length × Width × Height
A	2	Highlighting factor dynamic
B	$3/\max(\Delta)$	Highlighting factor gain

V. Results

Figure 8 shows the envelope (upper row), as well as the envelope with highlighting for the ROI in the area of the water-sediment transition at $z \approx 18 - 26\ \mathrm{cm}$ are shown (lower row) for each of the six burial positions of the object. In each case, a substantial magnitude is observed from the left edge obliquely to the lower right, which can be assigned to the reflection from one of the sidewalls of the aquarium. This occurs because the start position was chosen very close to the wall for the most extended possible travel in the aquarium. We also observe a typical crescent whose peak appears at a horizontal travel distance of $y \approx 20\ \mathrm{cm}$. This crescent is caused by the buried object or the object placed on the sediment. In the plots in the second row, the measured data were spectrally recalculated using the highlighting described in Section III. This attenuates parts of the reflection by the aquarium wall and the water-sediment transition and emphasizes signal components in the burial depth. The spectral characteristics caused by the buried object are identified by the post-processing at the vertical window in the burial depth and there the signal is highlighted. Whereas the signals outside the burial depth are decreased and the buried object is detectable.

The vertical burial position of the object is given by the light horizontal range in the lower row for each burial position. This lighted range is moving down slightly from the left position 1 to the right position 6 by $\approx 4\ \mathrm{cm}$, corresponding to the burial depths.

For the object in burial position 1, the crescent is strongly highlighted by the spectral post-processing, and the object can thus be detected and localized. In positions 2 to 6, the highlighting of the relevant area is shown, but not as strongly as before.

Finally, the measurements were performed without an object in the aquarium. In the first measurement, the edge, which was created when the object was removed, was not changed (see Figure 9 a). Afterward, the sediment was smoothed, and a second measurement was performed (see Figure 9 b).

In the upper Figure 9 the beginnings of the crescent, caused by the edge in the sediment, are observed. In the smoothed sediment in Figure 9 b these have disappeared. With spectral post-processing, the beginnings of the crescent in Figure 9 a are not further highlighted because the spectral patterns of the edge differ from those of the object. Compared to the post-processed images signals inside the ROI are not amplified strongly and the regions outside the ROI appear less attenuated, compared to the spectrally post-processed images in Figure 8. This shows that the spectral post-processing highlights the expected object. Crescents from different sources are not highlighted and surrounding parts of the ROI are not strongly attenuated, compared to the presence of an expected object.

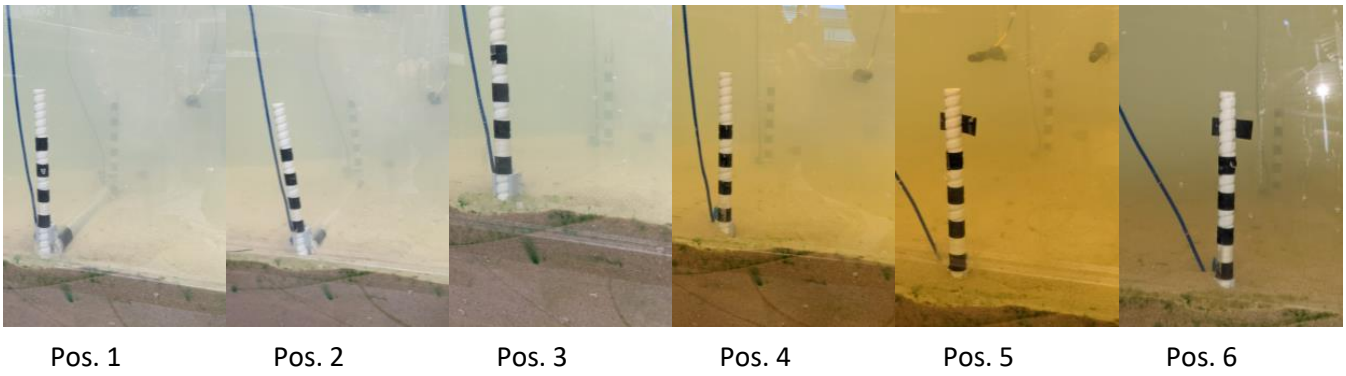

Figure 6. Measurement setup with object in 6 positions.

Figure 7. Test object that was buried.

VI. Conclusion and Future Work

This paper shows the extension of our underwater ultrasonic multipath model to highlight buried objects using spectral post-processing. A transformation geometrically adjusted the model to eliminate the direct LOS link between the transmitter and receiver since it does not temporally overlap with the other multipath components. The interferences between the temporally overlapping components of water-sediment reflection and diffraction around the buried object were thus isolated from the other components. The spectral pattern for this overlap and varying burial depths was then calculated using the model.

For evaluation, measurements were made in a laboratory setup in an aquarium with a hollow cylinder in different burial positions. In the area of the water-sediment transition, the measured data were compared spectrally with the model data using a fingerprinting procedure, and the object position was highlighted by spectral post-processing. Finally, the procedure was also performed on measurements without an object in the aquarium, and we could show that the object is detected and highlighted when present. In the absence, on the other hand, no unwanted artifacts appear in the ROI.

The presented method is suitable to detect and localize known object geometries in areas with multiple reflections. In our laboratory experiment, the object was already detectable even over the signal's envelope. It remains to be evaluated how objects that are barely visible in the envelope are detected spectrally. Furthermore, it has to be investigated how different objects can be spectrally distinguished from each other. Whether an additive superposition of our model consisting of cylinders is possible for more complex object geometries also remains to be evaluated in practice. For this purpose, it is also planned to use algorithms based on machine learning for pattern detection. Our model-based approach is suitable for the mass generation of required training data for AI algorithms.

With our spectral highlighting, we presented an additional method that assists in identifying objects buried in the sediment. The method is integrable into existing display and evaluation procedures independently of the transducers used, provided that the raw time-series data are available.

Acknowledgments

This publication results from the research of the Center of Excellence CoSA at the Technische Hochschule Lübeck and is funded by the Federal Ministry of Economic Affairs and Energy of the Federal Republic of Germany (Id 03SX467B, Project EXTENSE, Project Management Agency: Jülich PTJ). Horst Hellbrück is an adjunct professor at the Institute of Telematics of University of Lübeck.

References

[1] M. Stojanovic and J. Preisig, "Underwater acoustic communication channels: Propagation models and statistical characterization," *IEEE communications magazine*, vol. 47, no. 1, pp. 84–89, 2009.

[2] P. A. Van Walree, "Propagation and scattering effects in underwater acoustic communication channels," *IEEE Journal of Oceanic Engineering*, vol. 38, no. 4, pp. 614–631, 2013.

[3] T. Szyrowski, S. K. Sharma, R. Sutton, and G. A. Kennedy, "Developments in subsea power and telecommunication cables detection: Part 1-visual and hydroacoustic tracking." *Underwater Technology*, vol. 31, no. 3, 2013.

[4] D. B. Kilfoyle and A. B. Baggeroer, "The state of the art in underwater acoustic telemetry," *IEEE Journal of oceanic engineering*, vol. 25, no. 1, pp. 4–27, 2000.

[5] J. E. Piper, K. W. Commander, E. I. Thorsos, and K. L. Williams, "Detection of buried targets using a synthetic aperture sonar," *IEEE Journal of oceanic engineering*, vol. 27, no. 3, pp. 495–504, 2002.

[6] J. Wunderlich, G. Wendt, and S. Müller, "High-resolution echo-sounding and detection of embedded archaeological objects with nonlinear sub-bottom profilers," *Marine Geophysical Researches*, vol. 26, no. 2-4, pp. 123–133, 2005.

OCEANS Conference 2022 - Chennai

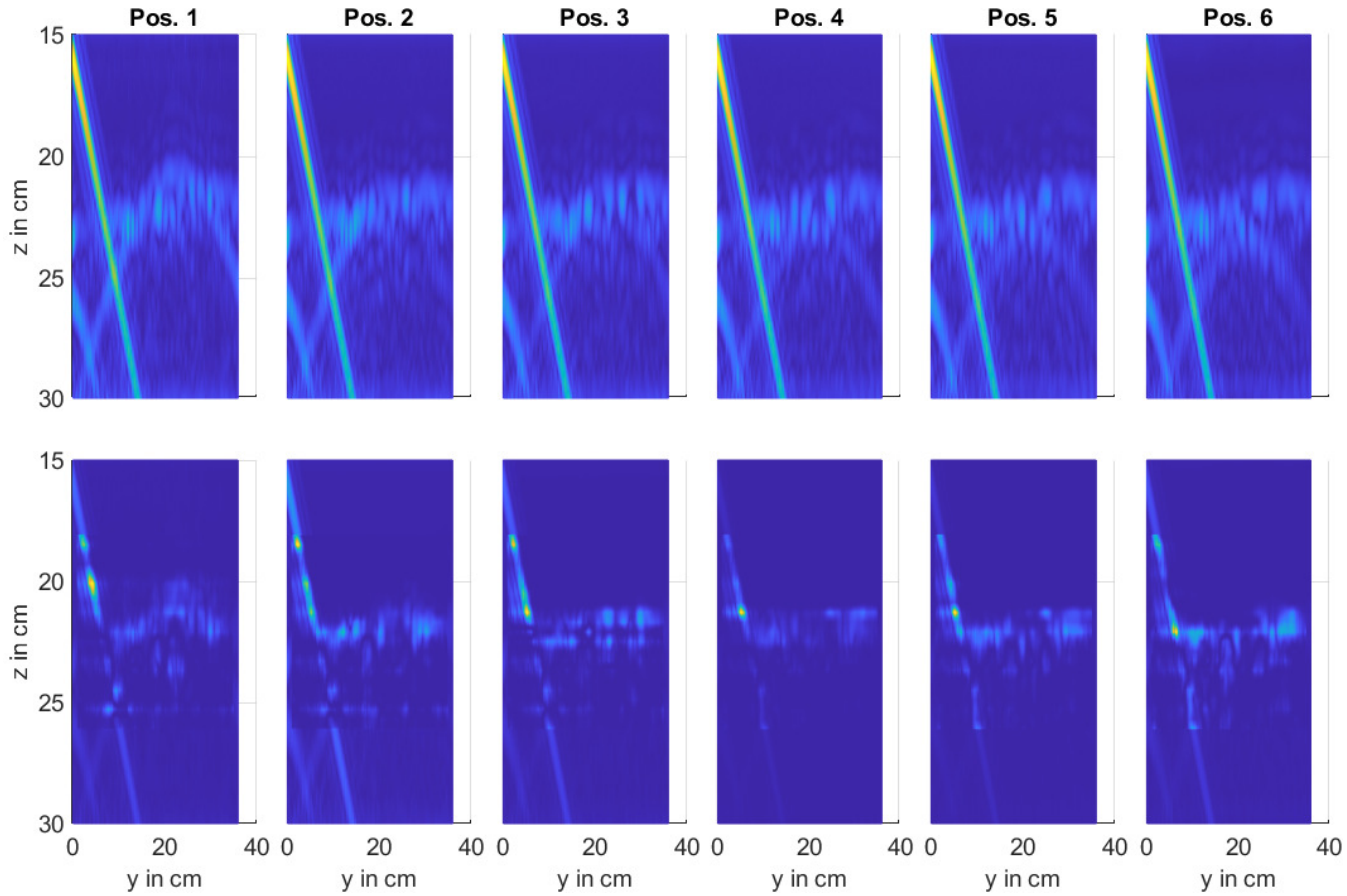

Figure 8. Measurement results with object in 6 positions (upper row: envelope; lower row: envelope highlighted with spectral processing).

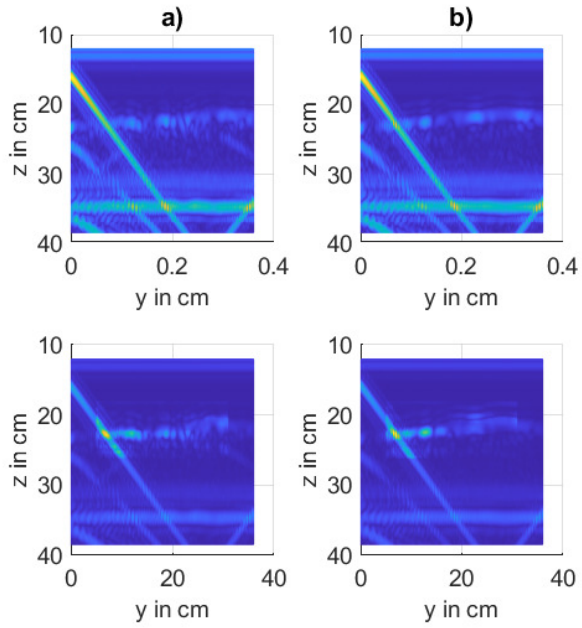

Figure 9. Measurement results for measurement without object for a) strong edge at sediment b) flat sediment surface.

[7] C. Capus, Y. Pailhas, K. Brown, and D. Lane, "Detection of buried and partially buried objects using a bio-inspired wideband sonar," in *OCEANS'10 IEEE SYDNEY*. IEEE, 2010, pp. 1–6.

[8] N. T. Hossain, R. M. Khan, and S. Rahman, "3-dimensional mapping of underwater surface for navigation using underwater ultrasonic piezoelectric transducer," Ph.D. dissertation, BRAC Univeristy, 2017.

[9] F. John, R. Kusche, F. Adam, and H. Hellbrück, "Differential ultrasonic detection of small objects for underwater applications," in *Global Oceans 2020: Singapore – U.S. Gulf Coast*, Oct 2020, pp. 1–7, https://ieeexplore.ieee.org/document/9389186. [Online]. Available: http://cosa.th-luebeck.de/download/pub/john-2020-differential-ultrasonic-oceans.pdf

[10] C.-W. Juan and J.-S. Hu, "Single-object localization using multiple ultrasonic sensors and constrained weighted least-squares method," *Asian Journal of Control*, 2021.

[11] L. Freitag, M. Johnson, and D. Frye, "High-rate acoustic communications for ocean observatories-performance testing over a 3000 m vertical path," in *OCEANS 2000 MTS/IEEE Conference and Exhibition. Conference Proceedings (Cat. No. 00CH37158)*, vol. 2. IEEE, 2000, pp. 1443–1448.

[12] T. Yang, "Properties of underwater acoustic communication channels in shallow water," *The Journal of the Acoustical Society of America*, vol. 131, no. 1, pp. 129–145, 2012.

[13] F. John, M. Cimdins, and H. Hellbrück, "Underwater ultrasonic multipath diffraction model for short range communication and sensing applications," *IEEE Sensors Journal*, vol. 21, no. 20, pp. 22 934–22 943, 2021.

[14] M. Cimdins, S. O. Schmidt, and H. Hellbrück, "Mampi-uwb—multipath-assisted device-free localization with magnitude and phase information with uwb transceivers," *Sensors*, vol. 20, no. 24, p. 7090, 2020.

[15] ——, "Modeling the Magnitude and Phase of Multipath UWB Signals for the Use in Passive Localization," in *16th Workshop on Positioning, Navigation and Communication*. IEEE, 2019.

[16] T. Li, H. Wang, Y. Shao, and Q. Niu, "Channel state information–based multi-level fingerprinting for indoor localization with deep learning,"

International Journal of Distributed Sensor Networks, vol. 14, no. 10, p. 1550147718806719, 2018.

[17] C. Capus, Y. Pailhas, K. Brown, J. Evans, and D. Willins, "Underwater detection classification and tracking using wideband sonar," in *Proceedings of the 3rd International Conference and Exhibition on Underwater Acoustic Measurements: Technologies & Results*, 2009.

[18] J. S. von Deimling, P. Held, P. Feldens, and D. Wilken, "Effects of using inclined parametric echosounding on sub-bottom acoustic imaging and advances in buried object detection," *Geo-Marine Letters*, vol. 36, no. 2, pp. 113–119, 2016.

[19] F. John, S. O. Schmidt, and H. Hellbrück, "High precision open laboratory 3d positioning system for automated underwater measurements," in *OCEANS 2021 San Diego – Porto*, 2021, pp. 1–5.

[20] ——, "Flexible arbitrary signal generation and acquisition system for compact underwater measurement systems and data fusion," in *OCEANS 2021 San Diego – Porto*, 2021, pp. 1–6.

[21] A. Roche, G. Malandain, X. Pennec, and N. Ayache, "The correlation ratio as a new similarity measure for multimodal image registration," in *International Conference on Medical Image Computing and Computer-Assisted Intervention*. Springer, 1998, pp. 1115–1124.

[22] *Hydrophone TC4013 - Miniature Reference Hydrophone*, http://www.teledynemarine.com/Lists/Downloads/RESON/Hydrophones/TC4013%20product%20leaflet.pdf, Teledyne Marine, 2020, accessed: 03.03.2021.